Biophysical Chemistry 12 (1980) 177–188

TORSION DYNAMICS AND DEPOLARIZATION OF FLUORESCENCE OF LINEAR MACROMOLECULES. II. FLUORESCENCE POLARIZATION ANISOTROPY MEASUREMENTS ON A CLEAN VIRAL ϕ29 DNA ☆

John C. THOMAS *, Stuart A. ALLISON, Carl J. APPELLOF and J. Michael SCHURR
Department of Chemistry, University of Washington, Seattle, WA 98195, USA

Received 9 April 1980

The decay of the fluorescence polarization anisotropy (FPA) of ethidium bromide bound to DNA has been studied over a range of time-spans from 18 ns to 120 ns with the aid of a picosecond dye laser. These FPA data have been fitted to three different functional forms: (1) the single-exponential-decay-plus-baseline employed by Wahl et al.; (2) the Initial Exponential Decay Zone formula of a recently developed rigid-rod and torsion spring model for the torsion dynamics of DNA; (3) the Intermediate Zone formula of that same model. At any fixed experimental time-span the formulas (2) and (3) provide slightly better fits than formula (1), but cannot be distinguished from each other by reduced chi-squared values alone. However, only the Intermediate Zone formula fits the data from all different time-spans with the same set of physical parameters. The parameters determined for formulas (1) and (2) vary with the time-span of the experiment in a characteristic manner that can be rationalized in the event that the FPA actually follows the Intermediate Zone curve. The fact that the torsion dynamics for this DNA is well described by the Intermediate Zone formula discounts the possibility of distinct widely spaced torsion joints in such clean DNAs. We are able to provide the first reliable value for the torsional rigidity of DNA, $C = 1.29 \pm 0.10 \times 10^{-19}$ dyne cm^2 in 0.01 M NaCl at 25°C.

1. Introduction

The decay of the fluorescence polarization anisotropy (FPA) of ethidium cation bound to DNA provides information about both the long-range torsional flexibility and the possible existence of localized mechanical inhomogeneities, or elastically weak torsion "joints", in the macromolecular filament [1]. Arguments presented earlier [1,2] demonstrate that in the time range accessible using ethidium dye, which has a lifetime of about 22 ns when bound to DNA, the depolarization of the fluorescence is essentially completely dominated by torsional Brownian motion about the local symmetry axis of the filament. In a previous paper [1], hereinafter referred to as I, a model consisting of a linear sequence of identical, rigid rods connected at their ends by torsion springs and undergoing coupled rotational Brownian motion about their fixed symmetry axes was proposed as a model for the torsion dynamics of DNA. An exact, though rather complicated, formulation was developed for the complete time-course of the decay of the FPA of dyes rigidly bound to that model.

The total time course of the relaxation can be divided into four characteristic time zones (i) the Initial Exponential Decay Zone, (ii) the Intermediate Zone, (iii) the Longest Internal Mode Zone; and (iv) the Uniform Mode Zone. The physical significance of the various zones is as follows. In the very early moments of the relaxation the elementary rod units rotate virtually independently of one another, so the initial decay of the FPA in this Initial Exponential Decay Zone is essentially that expected for rotational diffusion of uncoupled rods. Moreover, the decay rate is inversely proportional to the rod friction factor, or rod length, so that the individual rods are effectively "resolved" in this zone. At somewhat longer times such resolution of the uncoupled rod motions is no longer possible and the decay of the FPA is indistinguishable from that of an infinitely long continuum elastic filament.

☆ This work was supported in part by grants PCM 78-12136 and CHE-770-9131 from the National Science Foundation.
* Present Address: Department of Physics, University of Waikato, Private Bag, Hamilton, New Zealand.

This is the Intermediate Zone. At still longer times end-effects due to the finite length of the filament will become important. In other words, in this Longest Internal Mode Zone the extra depolarization of dyes attached near the free ends, where the amplitude of the torsional motions is much greater, will become important. Finally, the Uniform Mode Zone encompasses times so long that all of the higher internal modes have relaxed and only the uniform mode of rotation of the entire filament about its local symmetry axis contributes to the remaining depolarization. Simple approximate formulae are applicable in zones (i), (ii) and (iv).

The observed relaxations of the FPA of ethidium dye bound to either calf-thymus DNA ($M_r = 6.6 \times 10^6$)[3] or the present clean ϕ29 DNA ($M_r = 11.5 \times 10^6$) from 0–120 ns are incompatible with relaxations in zones (iii) and (iv). The Uniform Mode Zones of DNA's of such great length can be ruled out because their relaxation rates are much too slow to contribute on this time scale. The Longest Internal Mode Zones are also ruled out by an argument based on an inverse mismatch between the upper bound for the torsion constant imposed by the observed FPA at 120 ns and a lower bound arising from the requirement that the observed relaxation lie in zone (iii), as described for the calf-thymus DNA in sections 4 and 5 of paper I. In the case of the present ϕ29 DNA that inverse mismatch is even greater. Thus, the observed relaxation of the FPA of ethidium dye bound to these two DNA's must lie in either the Initial Exponential Decay Zone or the Intermediate Zone. Fortunately, for each of these zones a simple and accurate approximate formula is available for interpretation of the experimental data.

It was subsequently found [1] that the FPA *decay* data of Wahl et al. [3] for the calf-thymus DNA: ethidium cation complex could be equally well described by Initial Exponential Decay Zone behavior with a rod-length of 86 base-pairs, corresponding to widely spaced torsion joints, or by Intermediate Zone behavior with a rod-length of 1-base pair, corresponding to a torsionally uniform continuous elastic filament [2] over the accessible time-range of the experiment. That is, existing literature data for the relaxation of the FPA are inadequate to permit a distinction between these two possible torsion models. By employing *steady-state* FPA data [3] for the same complex in an extremely viscous, highly concentrated sucrose solution, a decision in favor of the model with torsion joints every 86 base-pairs could be made, assuming that the sucrose did not significantly perturb the elastic and frictional properties of the DNA. Such a conclusion remains contingent upon the validity of the FPA relaxation curve of Wahl et al., especially at times below 5 ns [1], where it is most difficult to obtain reliable data. Our motivation to search for torsion joints stems from dynamic light scattering experiments described in paper I and in forthcoming publications [4,5], wherein evidence is presented that bound contaminants, presumably basic proteins, present in commercial calf-thymus, and even some viral, DNA preparations profoundly influence the dynamics of internal Brownian motions at neutral pH, and also contribute to the titratable joint phenomenon at pH 10.2. The possibility that the native Watson-Crick structure might occasionally be interrupted by stretches of left-handed Z-helix [17,18] is also of considerable interest. Such a structural inhomogeneity would be expected to be associated with substantial alteration of the local torsion elastic properties, especially at the junctions between right- and left-handed helical domains.

The objective of the present work is to obtain for a clean viral DNA experimental data of sufficient precision at very short times that a decision between the two zones, or equivalently between torsion joints and torsional uniformity of that DNA, can be made, and to obtain the long-range torsion elastic constant of the filament.

We have studied the decay of the FPA of ethidium dye bound to ϕ29 DNA over a *range of time spans* from 18 ns to 120 ns at channel delays, or time resolutions, of 41 ps to 320 ps, respectively. The viral ϕ29 DNA used in this study has been the subject of extensive dynamic light scattering studies [4–7] and is known to possess no significant amount of adsorbed protein or polycation contaminants that are capable of inducing titratable joints of the kind mentioned above. The data have been analyzed using both the Initial Exponential Decay Zone formula and the Intermediate Zone formula of our model. For completeness the data have also been analyzed in terms of the simple single-exponential plus-baseline formula employed by Wahl et al. [3,8].

2. Materials and methods

2.1. DNA samples

Concentrated stock solutions of DNA (~2 mg ml^{-1} DNA) were prepared in the manner described previously [4]. For the FPA measurements the DNA was simply diluted to 0.05 mg ml^{-1} with 10^{-2} M NaCl solution containing ethidium bromide at a concentration of 0.10 μg ml^{-1}. The pH of the final solution was 7.2.

Under these conditions the ratio of the molar DNA phosphate concentration to the molar dye concentration, the P/D ratio, is ~600. This value of P/D is ~5 times larger than for any previous studies and insures that decay of the FPA due to the energy transfer between dye molecules is completely negligible [8].

2.2. Fluorescence anisotropy measurements

2.2.1. Experimental apparatus

These measurements were carried out using a picosecond pulsed dye laser and time-correlated single-photon-counting detection. Fig. 1 is a schematic of the experimental apparatus. The Spectra-Physics picosecond dye laser consists of a mode-locked Ar^+ laser synchronously pumping a cavity-dumped dye laser.

Operation of the system is as follows: the output of the dye laser passes through the beam-splitter BS, a UV-grade prism polarizer P_1, a polarization rotator PR and finally enters the sample cell C containing the fluorophore solution. The sample cell is enclosed in a housing with both entrance and exit apertures (as well as a side-view aperture) so that the unabsorbed laser beam can be dumped. The resulting fluorescence signal is viewed at right angles to the incident beam direction. The fluorescent light passes through the 630 nm cut-on filter,F, a similar polarizer P_2, a monochromator (Bausch and Lomb 0.25 meter) and is finally detected by the photomultiplier tube PM.

Output pulses from the photomultiplier tube (an RCA 31034 operating at 2200 V in a thermoelectrically cooled housing) are amplified and then input to an Ortec 934 constant-fraction discriminator (CFD) the output of which serves as the START pulse for the Ortec 457 biased time-to-ampitude converted (TAC). The beam splitter directs a portion of the incident laser pulse into the photodiode PD (an HP5082-4203 operating at −90 V bias with a rise time <1 ns). The output of the photodiode, after appropriate constant-fraction discrimination and delay is used as the STOP pulse for the TAC. This "inverted" mode of operation increases the throughput rate of the TAC by ensuring that the TAC is only ever started when a photon has been detected, thus eliminating dead-time due to "time-out" which occurs in the conventional TAC configuration (i.e. START and STOP reversed from the configuration in fig. 1), when no photon is detected (i.e. most of the time) [9].

Finally the TAC output is input to a Tracor Northern TN-1705 pulse height analyzer (PHA), which builds up to the histogram of photon arrival times, which, of course, is just the fluorescence response of the system. The PHA is interfaced to a TERAK/LSI-11 microcomputer which transfers the data onto floppy disc and performs curve-fitting on the experimental data.

The two polarizers and the polarization rotator are essential to measure the polarization components (vertical and horizontal) of the fluorescence intensity. Both P_1 and P_2 are aligned to be precisely parallel to the initial laser polarization (i.e. vertical) and the required polarization component is then selected by rotating the plane of polarization of the incident light with the polarization rotator; 0° rotation gives the vertical component and 90° rotation the horizontal component. To measure "rotation-free" fluorescence lifetimes the initial beam polarization is rotated by 54.7°. This scheme has the particular advantage that the light-incident on the monochromator always has the same polarization (vertical) and the well-known problem of the polarization dependence of the monochromator transmission coefficient is thus eliminated.

All experiments described here were done with rhodamine 6G as the lasing medium for the dye-laser and the cavity-dumping rate was 800 kHz. All measurements were made with the dye-laser tuned in the range 575–585 nm and the fluorescence was monitored at 650 nm. In addition, to ensure single-photon statistics and eliminate distortion due to pulse pile-up, the monochromator slits were closed down to give a photon detection rate which was less than 10% (usually ~1%) of the cavity-dumping rate [10]. The dye-laser pulse width was measured to be ≤15 ps using the technique of background-free correlation by second harmonic generation [11] and the full-width half-maximum of the photomultiplier tube in response to these

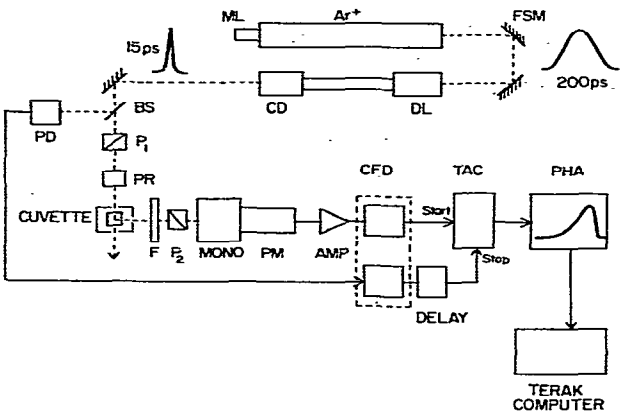

Fig. 1. Picosecond laser and single-photon counting system. ML: mode-locker, Ar^+: argon ion laser, FSM: front surface mirror, DL: dye laser, CD: cavity-dumper, BS: beam splitter, PD: photodiode, P_1, P_2: prism polarizer, PR: polarization rotator, F: red filter, MONO: monochromator, PM: photomultiplier tube, CFD: constant-fraction-discriminator, TAC: time-to-amplitude converter, PHA: pulse height analyzer.

pulses was 580 ps. All experiments were performed at room temperature, 25 ± 1°C.

2.2.2. Fluorescence components

The measured vertical and horizontal polarization components of the fluorescence intensity, $i_V(t)$ and $i_H(t)$ respectively, can be combined to form the following two experimental decay curves,

$$s(t) = i_V(t) + 2i_H(t), \quad d(t) = i_V(t) - i_H(t).$$

$s(t)$ and $d(t)$ are related to the true decay curves $S(t)$ and $D(t)$ by the usual convolution relations,

$$s(t) = \int_0^t e(t')S(t-t')\,dt', \tag{2a}$$

$$d(t) = \int_0^t e(t')D(t-t')\,dt'. \tag{2b}$$

Here $e(t)$ is the apparatus response function, which is determined by recording the decay function with a diffuse scatterer in place of the fluorophore solution. Note that, as $e(t)$ is measured at the excitation wavelength and $s(t)$ and $d(t)$ are measured at a different (longer) wave length, care must be taken that $e(t)$ is not distorted by the wavelength dependence of the photomultiplier tube response. For instance we have found that for an RCA 8850 phototube its response is shifted to longer times *and* its pulse-shape changes as the wavelength of the incident light goes from 580 nm to 640 nm. However, the RCA 31034, which was used in the present experiments, has much greater red sensitivity and a broader spectral range than the 8850 and has been found to be free of such wavelength-dependent behavior.

The fluorescence polarization anisotropy $r(t)$ is simply the ratio of the difference and the sum of the two polarization components i.e.

$$r(t) = D(t)/S(t). \tag{3}$$

This relationship plus eq. (2b) gives

$$d(t) = \int_0^t e(t')r(t-t')S(t-t')\,dt'. \tag{4}$$

The scheme for analyzing the anisotropy decay is then as follows:

1) measure $i_V(t)$, $i_H(t)$ and $e(t)$ (for the same number of laser "shots");

2) calculate (point by point) $s(t)$ and $d(t)$;

3) determine $S(t)$ by fitting the $s(t)$ data to a convolution of $e(t)$ and an exponential decay (or sum of exponential decays);

4) using $S(t)$ determined in 3) fit the $d(t)$ data to a convolution of $e(t)$ and the product $r(t)S(t)$ to determine the best-fit parameter values for the particular model chosen for $r(t)$.

Curve-fitting is carried out on the TERAK/LSI-11 using a convolute-and-compare approach with our locally written non-linear least-squares FORTRAN program which is based on the Marquardt algorithm [12]. For the special case (i.e. $S(t)$) when the functional form was simply a convolution of the instrument response and a sum of exponentials, a huge reduction in computing time was achieved using the recursion relations for the function and its derivatives given by Grinvald and Steinberg [13]. In this case a sum of exponentials could be fitted in about 90 seconds or less. When the fitting involved more complex forms for which recursion relations were not available, the data fitting typically took 20 minutes or more. Several (3–4) complete data sets were measured and fitted for each experimental time-span.

2.3. Models for r(t)

The following expression for the fluorescence polarization anisotropy was given in paper I,

$$r(t) = r_0 \{a_1 + a_2 g(t) + a_3 g(t)^4\}, \quad (5)$$

where

$$a_1 = (\tfrac{3}{2}\cos^2\epsilon - \tfrac{1}{2})^2, \qquad a_2 = 3\sin^2\epsilon\cos^2\epsilon,$$

$$a_3 = \tfrac{3}{4}\sin^4\epsilon,$$

and $\epsilon = 70.5°$ is the constant angle between the transition dipole moment of the ethidium cation and the local helix axis. The initial decay amplitude r_0 has a maximum value of 0.4. Approximate formulae for the correlation function $g(t) \equiv \langle \exp\{-i[\phi(t) - \phi(0)]\}\rangle_{T,R}$ (where $\phi(t)$ denotes the instantaneous torsion angle of a rod, and the subscripts T,R denote averages over all trajectories (T) of the system, and all rods (R) to which the dye might bind) were given in paper I for the two relaxation zones of interest.

2.3.1. Initial exponential decay zone

$$g(t) = \exp\left[\frac{-k_B T}{\alpha}\,\frac{\alpha t/\gamma}{1+\alpha t/\gamma}\right]; \quad \alpha t/\gamma < 1, \quad (6)$$

where α is the torsion spring constant between rods and γ is the friction factor for azimuthal rotation about the symmetry axis of the rod. k_B is the Boltzmann constant and T is the absolute temperature.

In this case data for the various channels $n = 0, 1, 2, \ldots$ of the pulse height analyzer were fitted to an expression of the form

$$r(n) = r_0\left[a_1 + a_2 \exp\left(-\frac{n}{C_1 + D_1 n}\right) + a_3 \exp\left(-\frac{4n}{C_1 + D_1 n}\right)\right], \quad (7)$$

wherein r_0,

$$C_1 = \gamma/\Delta t\, k_B T, \quad D_1 = \alpha/k_B T, \quad (8)$$

were treated as adjustable parameters. The channel delay time Δt is a known experimental constant for any particular data set. Because the Initial Exponential Decay Zone formula is expected to be always valid on some sufficiently short time-scale, it is anticipated that eq. (7) should provide the least satisfactory fit to the long time-span data, and become increasingly better as the time-scale is reduced, provided that this zone is actually accessible to a substantial fraction of the data channels at the shorter time-spans. We return to this point subsequently.

We have generally assumed that γ may be computed for a rod of any given length using Perrin's result [14] for cylinders, which can be expressed in the form

$$\gamma = \gamma_0 p \quad (9)$$

where $\gamma_0 = 4\eta\pi a^2 h = 5.47 \times 10^{-23}$ dyne cm s is the fraction factor of a short cylinder 3.4 Å long and 12 Å in radius, corresponding to 1 base-pair, and p is the number of base-pairs in one rod, or between torsion joints, in the model. Clearly, an experimental determination of C_1 would permit evaluation of p, whereas D_1 would permit evaluation of the torsion elastic constant α.

2.3.2. Intermediate zone

$$g(t) = \exp[-k_B T(t/\pi\alpha\gamma)^{1/2}]; \quad (\alpha t/\gamma) \gtrsim 1/4. \quad (10)$$

The peculiar $\sqrt{t}$ dependence of the argument of this exponential function is characteristic of this zone. In this case the data were fitted to

$$r(n) = r_0[a_1 + a_2 \exp(-C_2\sqrt{n}) + a_3 \exp(-4C_2\sqrt{n})], \quad (11)$$

wherein both r_0 and

$$C_2 \equiv \frac{k_B T}{(\pi\alpha\gamma)^{1/2}}(\Delta t)^{1/2}, \quad (12)$$

were treated as adjustable parameters. For a given *long-range* torsional rigidity and friction factor per unit length the product $\alpha\gamma$ is independent of the number of base pairs p in the elementary rod (which cannot be resolved in this zone), because $\gamma = \gamma_0 p$ and $\alpha = \alpha_0/p$, where γ_0, α_0 apply for $p = 1$ base-pair. Determination of C_2 then permits evaluation of α_0, provided γ_0 can be accurately estimated from Perrin's formula above.

2.3.3. Single exponential decay plus baseline

For the single-exponential-plus-baseline formula of Wahl et al. [3,8] the data were simply fitted to the form

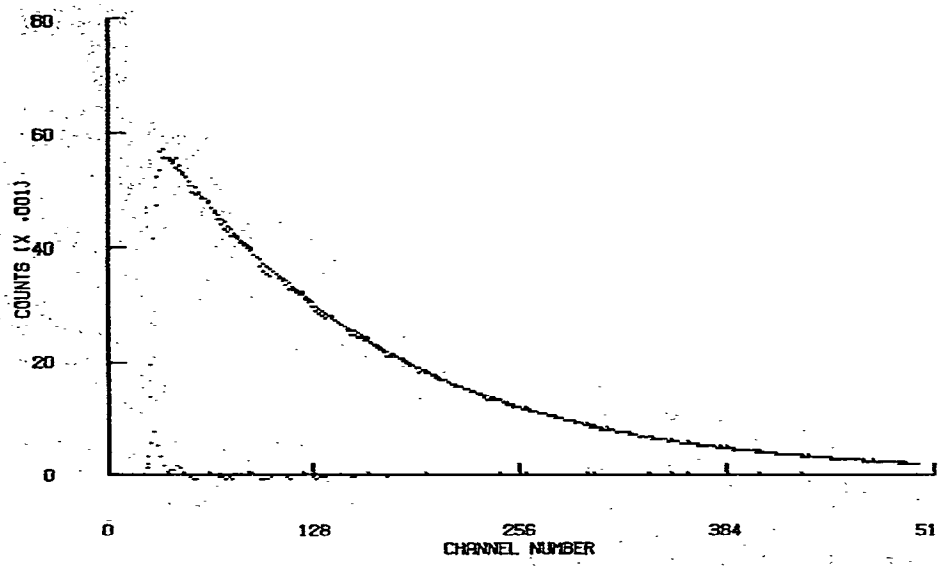

Fig. 2. The sum fluorescence response $s(t)$ on a timescale of 0.1599 ns/channel. The best-fit single exponential (convoluted with the instrument response) gives a lifetime of 22.2 ns. The differences between the data and the fitted curve can be seen scattered about zero.

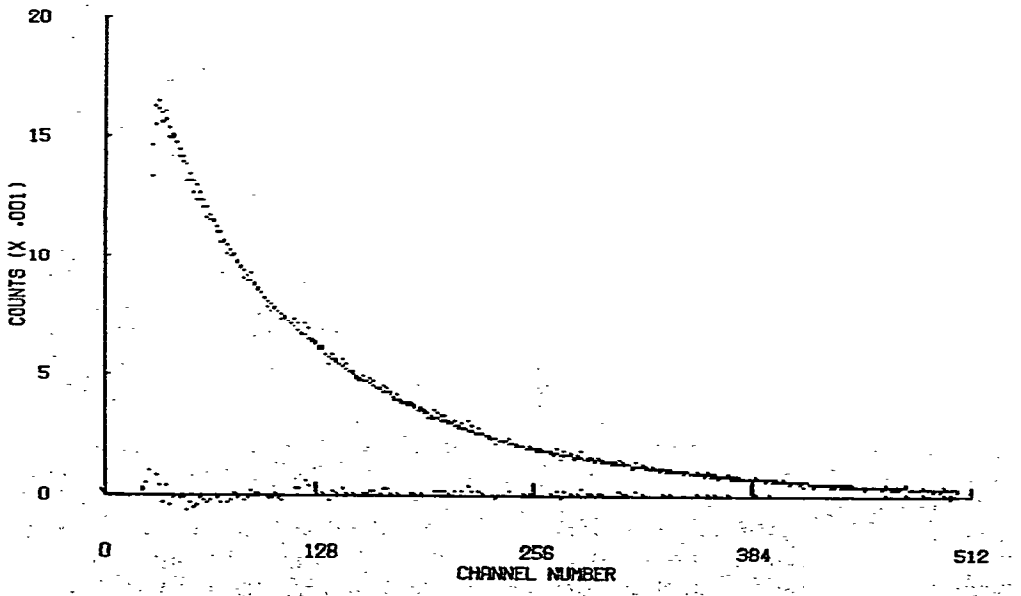

Fig. 3. The difference fluorescence response $d(t)$ and the best-fit curve using the Initial Exponential Decay Zone eq. (7) for $r(t)$. Time-scale: 0.1599 ns/channel. The lower curve is the difference between the data and the best-fit curve.

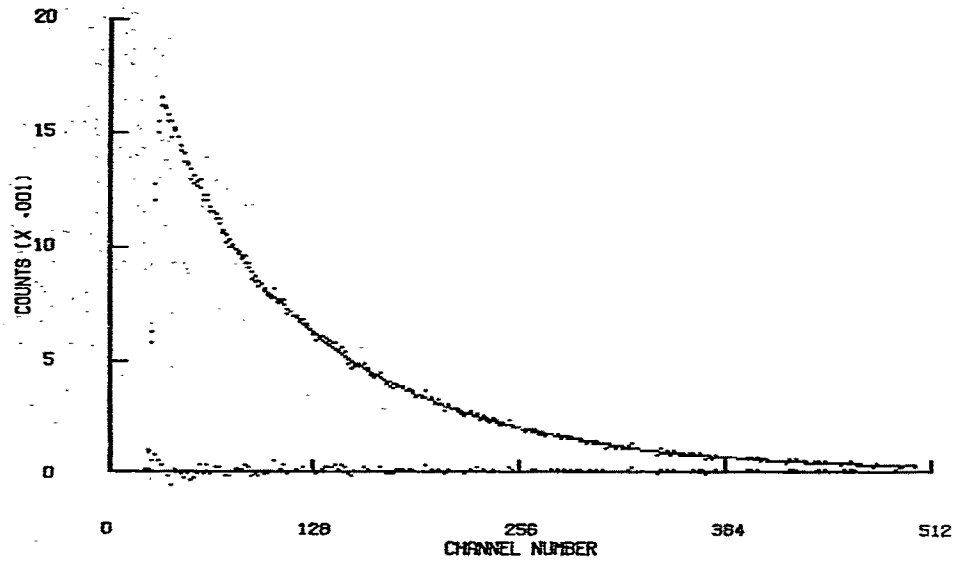

Fig. 4. The difference fluorescence response $d(t)$ and the best-fit curve using the Intermediate Zone eq. (11) for $r(t)$. The lower curve is the difference between the data and the best-fit curve. Timescale: 0.1599 ns/channel.

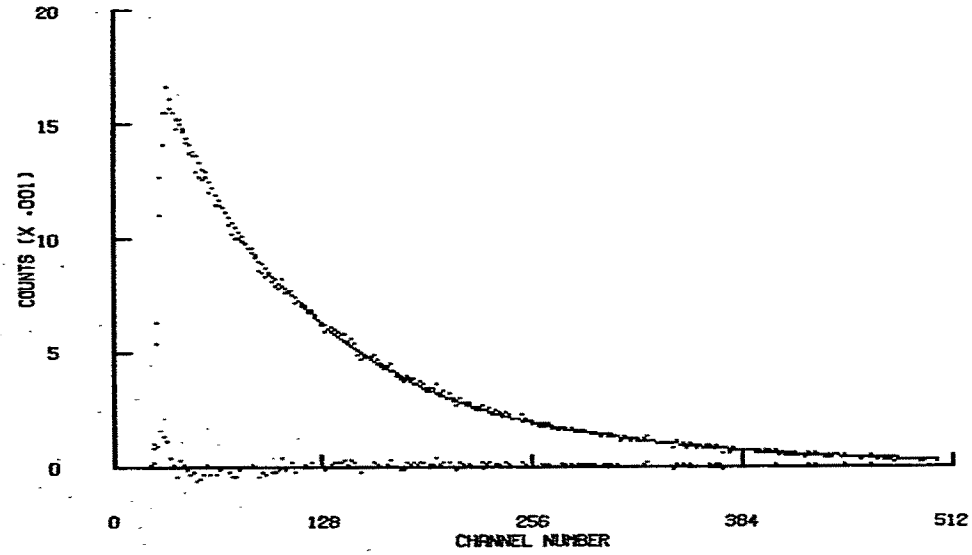

Fig. 5. The difference fluorescence response $d(t)$ and the best-fit curve using the single-exponential-plus-baseline eq. (13) for $r(t)$. The lower curve is the difference between the data and the best-fit curve. Timescale: 0.1599 ns/channel.

$$r(n) = A_1 \exp[-C_3 n] + A_2, \quad (13)$$

wherein A_1, A_2 and

$$C_3 \equiv \Delta t/\tau \quad (14)$$

were treated as adjustable parameters, and τ is the relaxation time.

3. Results and discussion

Fig. 2 is a representative plot of the sum data $s(t)$ along with the best-fit single exponential (convoluted with the instrument response) on a time scale of 0.1599 ns/channel. The figure is simply a bit-mapped facsimile of the computer display and due to the limited resolution of the graphics system (320 × 240) only every second datum point appears on the figure. Note that, for the same reason, the data are substantially smoother than it would appear from the graph (this is particularly true out on the "tail" of the curve). The differences between the experimental data and the fitted curve are also shown on the figure and it can be seen that they are reasonably evenly scattered around zero indicating a good fit to the experimental data. The exponential relaxation time, which is just the fluorescence lifetime of the ethidium bromide dye, is 22.2 ns. Furthermore, over the entire range of time-spans (0–18 ns to 0–120 ns), or respective channel delays (41–320 ps), investigated the sum data gave relaxation times that were within 7% of this value.

A plot of the corresponding difference data $d(t)$ is presented in figs. 3, 4 and 5 along with the best fits to those data using eq. (4) with $r(t)$ described by eqs. (7), (11), and (13), respectively. Evidently, all three formulae represent this particular data set rather well, although it is notable that the single-exponential-plus-baseline equation (13) does not give quite as good a fit at short times. The question now arises as to which representation of $r(t)$ most faithfully describes the decay of the FPA. The question is answered by considering:

i) the "goodness-of-fit" for each formula, as measured by the reduced chi-squared values (χ^2_ν);

ii) the variation of the best-fit model parameters with the time-span of the experiment.

3.1. χ^2_ν values

The χ^2_ν values obtained were generally comparable for eqs. (7), (11) and (13). However, except for the shortest time-span, lower values were consistently observed for eqs. (7) and (11) than for eq. (13). For example, the χ^2_ν values in figs. 3, 4, and 5 are 8.0, 6.2, and 9.7, respectively. This indicates that the Initial Exponential Decay Zone and Intermediate Zone formulae actually provide a superior fit to the data. Although the χ^2_ν values for eqs. (7) and (11) were generally quite close on all time scales, it must be noted that the former Initial Exponential Decay Zone formula contains 3 adjustable parameters, whereas the latter Intermediate Zone formula contains only 2.

It is notable that these reduced chi-squared values are much larger than that ($\chi^2_\nu \approx 1.0$) expected when the functional form is a good representation of the data, and when the standard deviation of the data is independently known, as we believe it is in this case of simple Poisson photon statistics [12]. However it is obvious that the fits to the data are much better than the χ^2_ν values imply, except for the aforementioned significant deviations in the first few channels, which evidently are the source of these anomalously large χ^2_ν values. We believe that this systematic deviation in the very early channels is due to a very small intermittent timing jitter (<40 ps) in the TAC/PHA combination and to the detection of both stray light and Raman scattered light that are transmitted through the monochromator. Such light is not convoluted with the response of the dye, and is therefore not properly accounted for in the curve-fitting procedure.

3.2. Variation of model parameters with experimental time-span

Figs. 6, 7 and 8 summarize the results of experiments performed over the different time-spans, which were varied simply by changing the indicated channel delay. Each point is the average of three to four measurements. In fig. 6 the two parameters C_2 and r_0 of the Intermediate Zone eq. (11) are plotted against the square-root of the channel delay $(\Delta t)^{1/2}$. Two things are immediately apparent from this figure.

i) C_2 is very nearly proportional to $(\Delta t)^{1/2}$ in concordance with eq. (12).

ii) The initial anisotropy is in the range $0.325 \gtrsim r_0$

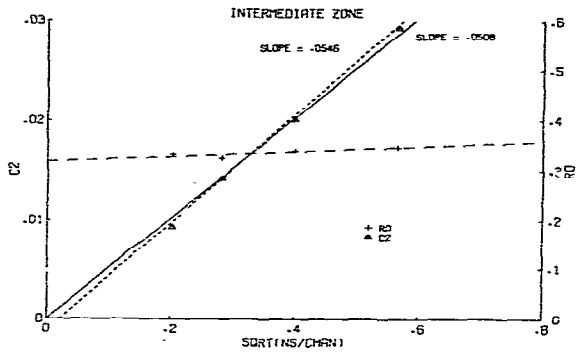

Fig. 6. Variation of the best-fit parameters C_2 (△) and r_0 (+) for the Intermediate Zone eq. (11) with experimental time-span. Note that the parameters are plotted against the *square-root* of delay time per channel (i.e. $\Delta t^{1/2}$). Each point represents the average value obtained from 3–4 experiments at a given channel delay-time.

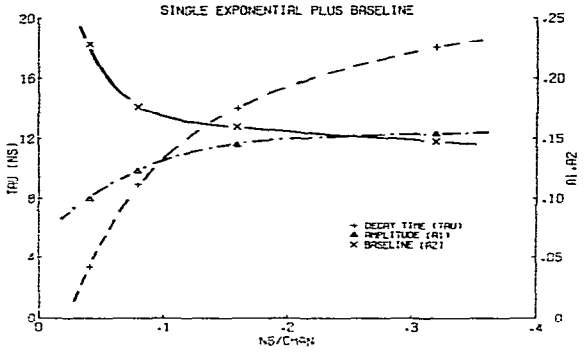

Fig. 8. The three-best-fit parameters A_1 (△), A_2 (×) and τ (+) for the single-exponential-plus-baseline eq. (13) as a function of delay time per channel, or equivalently the experimental time-span. Note that in this case the abscissa is simply Δt. Each point represents the average value obtained from 3–4 experiments at a given channel delay time.

$\lesssim 0.345$ and changes very little as the experimental time-scale is varied from 18 ns to 120 ns, in accord with eq. (11).

The three best-fit parameters r_0, α and γ of the Initial Exponential Decay Zone eqs. (7) and (8) are plotted versus channel delay Δt in fig. 7. It is immediately apparent that γ and α are not constant, as required by the physical model. Specifically, α increases and γ decreases, both in a pronounced and progressively steepening manner, as the time-span of the experiment is decreased. Evidently, the Initial Exponential Decay Zone formula cannot adequately describe the decay of the FPA data over the complete range of time-spans with a *fixed* set of parameters α and γ. Moreover, this failure is obviously exacerbated by decreasing the time-span of the experiment, which would have been expected to improve the validity of the Initial Exponential Decay Zone, if that zone were actually accessible to a substantial fraction of the data channels, as noted above.

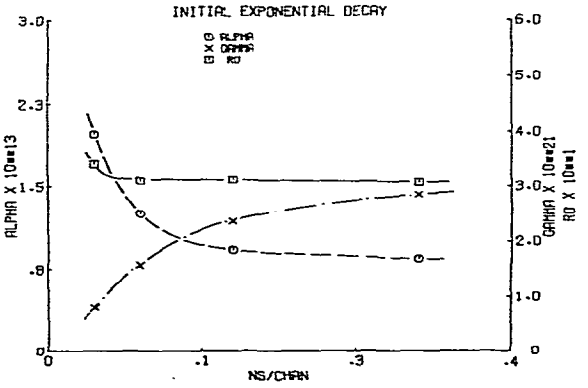

Fig. 7. The three best-fit parameters r_0, α and γ for the Initial Exponential Decay Zone eqs. (7) and (8) as a function of delay time per channel, or equivalently the experimental time-span. Note that in this case the abscissa is simply Δt. Each point represents the average value obtained from 3–4 experiments at a given channel delay time.

The three best-fit parameters A_1, A_2 and τ for the single-exponential-plus-baseline eq. (13) are shown as a function of Δt in fig. 8. It is seen that these parameters all vary markedly in a non-linear way with the time-span of the experiment. Specifically, as the experimental time-span is reduced, the exponential decay time τ and amplitude A_1 decrease dramatically, whilst the baseline undergoes a complementary increase. Evidently, this formula cannot adequately describe the decay of the FPA data over the complete range of time-spans with a *fixed* set of the parameters A_1, A_2 and τ.

The success of the Intermediate Zone formula and the failure of both Initial Exponential Decay Zone and single-exponential-plus-baseline formulas are demon-

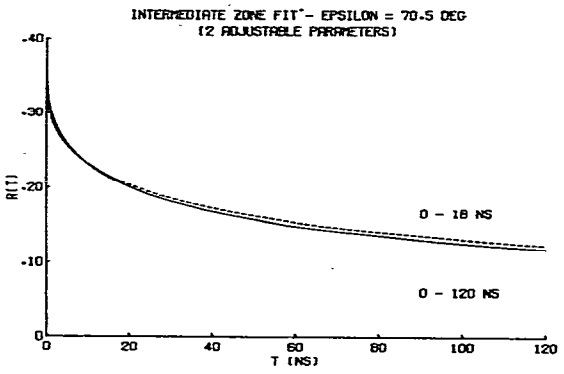

Fig. 9. Predicted behavior of $r(t)$ for the Intermediate Zone eq. 11. $r(t)$ is reconstructed from the best-fit parameters obtained from the two extreme time-spans (0–18 ns and 0–120 ns). The broken line is the extrapolation of the 18 ns curve to 120 ns. Note the close agreement between the two curves.

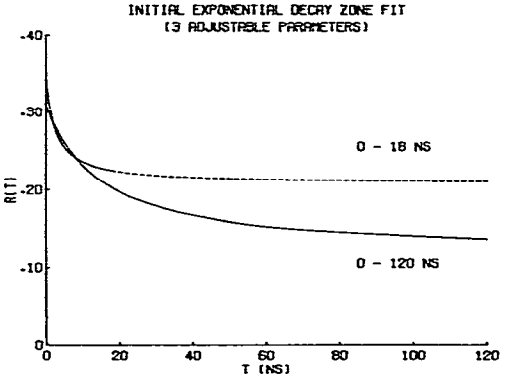

Fig. 10. Predicted behavior of $r(t)$ for the Initial Exponential Decay Zone eq. (7). $r(t)$ is reconstructed from the best-fit parameters r_0, α and γ obtained from the two extreme time-spans (0–18 ns and 0–120 ns). The broken line is the extrapolation of the 18 ns curve to 120 ns. Note the large disparity between the two curves.

strated conclusively in figs. 9, 10 and 11. Here we have reconstructed $r(t)$ using the best-fit parameters of all three formulae for the two extreme experimental time-spans, viz. 0–18 ns and 0–120 ns. The broken lines are obtained by extrapolating the 18 ns curves out to 120 ns. For the Intermediate Zone essentially the same $r(t)$ curve is obtained using the best-fit parameters from either the short or long time span data (fig. 9), whereas for both the Initial Exponential Decay Zone and single-exponential-plus-baseline formulae the short and long time-span parameters give radically different decay curves (figs. 10 and 11).

The limiting slope of the Intermediate Zone formula (eq. (11)) rises to infinity at $t = 0$, and its curvature likewise diverges at $t = 0$. Clearly, when the data actually fall in the Intermediate Zone, the best-fit single-exponential-plus-baseline curves would be expected to show decreasing relaxation times and amplitudes, and also increasing base-lines with any decrease in experimental time-span, and these trend should accelerate at the shorter time-spans, as observed in fig. 8. Likewise, the failure of the Initial Exponential Decay Zone formula would be expected to become progressively more severe, in the sense that the best-fit γ, which governs the initial exponential relaxation time, would undergo an accelerating decrease, and α, which governs the apparent plateau at long times, should undergo an accelerating increase with decreasing experimental time-span, as observed in fig. 7. Thus, the variation of the fitting "results" for all of the formulas (7), (11) and (13) with the experimental time-span can be rationalized under the premise that the data fall in the Intermediate Zone.

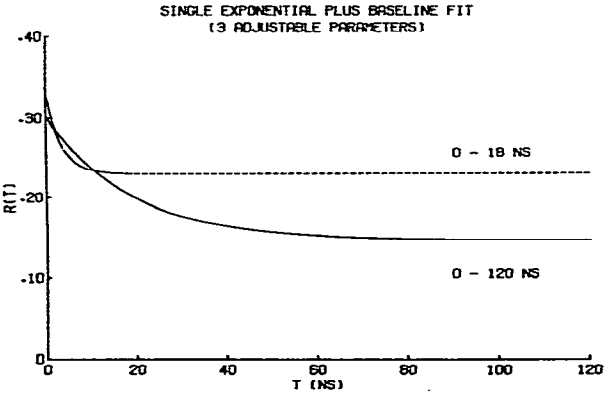

Fig. 11. Predicted behavior of $r(t)$ for the single-exponential-plus-baseline eq. (13). $r(t)$ is reconstructed from the best-fit parameters obtained from the two extreme time-spans (0–18 ns and 0–120 ns). The broken line is the extrapolation of the 18 ns curve to 120 ns. Note the large disparity between the two curves.

3.3. DNA torsion constant

The slope of the C_2 versus $(\Delta t)^{1/2}$ plot in fig. 6 gives a very reliable value for the torsion constant α of the Hookean springs connecting the rods in the DNA. The broken curve depicts the best-fit straight line to the data whilst the solid curve is a similar fit, but in this case the straight line is constrained to pass through the origin. The slopes of these two curves, 0.055 and 0.051, respectively, differ by less than 8%.

Squaring both sides and rearranging eq. (12) gives

$$\alpha = \frac{k_B^2 T^2}{\pi\gamma} \frac{\Delta t}{C_2^2} \tag{15}$$

Using the value $\gamma_0 = 5.5 \times 10^{-23}$ dyne cm s for a rod of length 1 base-pair (c.f. eq. (9)) and the smaller value of the slope $(C_2/(\Delta t)^{1/2})$ obtained above gives

$$\alpha = (3.8 \pm 0.3) \times 10^{-12} \text{ dyne cm} \tag{16}$$

at 25°. Making use of the relation $C = \alpha h p$ [1], where $h = 3.4 \times 10^{-8}$ cm is the rise per base-pair along the DNA, and $p = 1 = 1$ base-pair per rod, as assumed in computing γ_0, there results

$$C = 1.29 \pm 0.10 \times 10^{-19} \text{ dyne cm}^2 \tag{17}$$

for the long-range torsional rigidity of this $\phi 29$ viral DNA in 10^{-2} M NaCl at 25°C. This value is the first accurate experimental estimate of the torsion elastic constant for DNA, or indeed for any macromolecule.

The twist energy parameter is given in paper I as $U(2\pi\tau, N)N/(k_B T \tau^2) = C 2\pi^2/(hk_B T)$, where $U(2\pi\tau, N)$ is the torsion energy required to introduce τ complete twists into an *axially fixed* DNA segment of N base-pairs. In the present case it has the value

$$U(2\pi\tau, N)N/(k_B T \tau^2) = 1821, \tag{18}$$

which lies significantly below the value 2541 estimated using the Intermediate Zone torsional rigidity $C = 1.77 \times 10^{-19}$ obtained from the data of Wahl et al. for calf-thymus DNA at 20°C in paper I. Whether this discrepancy is attributable to a real difference in the DNA's studied, or to errors inherent in the data of Wahl et al. is not known at the present time. In any event the value in eq. (18) still exceeds all of the measured [15,16] free-energy parameters $F(\tau, N)N/(k_B T \tau^2)$ where $F(\tau, N)$ is the free-energy required to introduce τ superhelical coils (actually topological twists) into a DNA segment of N base-pairs, which parameters generally lie in the range 1070 ± 150, except for one plasmid DNA that gives anomalously high values from 1390–1560 [15]. It may be concluded that the axial bending deformation associated with the tertiary turns acts to substantially relieve the torsion strain energy that would otherwise be required to introduce these topological twists into a given segment of DNA.

3.4. Physical significance of the intermediate zone

Our conclusion that the data fall in the Intermediate Zone implies that this DNA behaves essentially as a torsionally smooth continuous elastic filament. It is obvious, however, that sufficiently closely spaced torsion joints could have escaped detection, and likewise that very widely spaced torsion joints also would not have been detected, so it is worthwhile to comment on the probable limits placed on joint spacing, or rod-length, by these experiments.

The best-fit value of γ for the Initial Exponential Decay Zone at the shortest time-span is $\gamma = 0.79 \times 10^{21}$ dyne cm s, which in view of eq. (9) gives $p = 15$ base-pairs for the apparent elementary rod-length. If, in fact, the rod-length were $p \approx 20$ base-pairs, or greater, then the γ and α values should have begun to flatten out on the shortest time-span, rather than continuing their accelerating trends. Rod lengths much shorter than $p \approx 20$ base-pairs would probably not have produced sufficient Initial Exponential Decay Zone behavior to alter these trends even at the shortest time-span. The long-time limit of the Initial Exponential Decay Zone is determined (from $\alpha t/\gamma < 1$) to be $t \leqslant 4$ ns. Thus, rod-lengths much less than about $p \approx 20$ base-pairs would not have been detected in these experiments.

The maximum distance between torsion joints that could have been detected in these experiments is more difficult to estimate with precision, because the answer obviously depends on how weak is the torsion constant at the joint in comparison to the α that we have just measured, which presumably applies only to the uniform region between joints. If the joints were to exhibit torsion constants that are negligibly small compared to α, then the torsion dynamics would be essentially just that of unconnected uniform segments of DNA of a length equal to the interjoint spacing. As shown in paper I, the observations should begin to deviate from Inter-

mediate Zone behavior when $t = 120$ ns $\geq \tau_{11}$, the relaxation time of the 11th normal mode of the interjoint DNA segment, which is given approximately by $\tau_{11} = \gamma_0(n+1)^2/100\alpha\pi^2$ (c.f. eq. (28) of I), where $n+1$ is the number of base-pairs between joints. Using γ_0 from eq. (9) and α from eq. (16) one finds the criterion $(n+1) \lesssim 2870$ for the onset of significant end-effects in the short segments between joints, which would be expected to produce downward deviations of the FPA from the Intermediate Zone curve. Allowing for a finite α at the torsion joints, a more conservative figure of $(n+1) \lesssim 1000$ base-pairs is probably justified. That is, joints farther apart than 1000 base pairs would likely have escaped detection, while those closer than 1000 base-pairs should have produced significant deviations from the Intermediate Zone formula.

In summary, the present data indicate that the linear density of torsion joints cannot lie in the range from 1 in every 20 base-pairs to roughly 1 in every 1000 base-pairs. This indicates that the present clean ϕ29 DNA does not contain locally denatured regions within this linear density range, nor does it within the same limits bear bound protein contaminants that substantially alter its local elastic properties, in general agreement with the dynamic light scattering results [4,5]. The present data also provide a strong, but not absolutely conclusive, argument that regions of Z-helix do not occur within the stated range of linear densities in the present ϕ29 DNA. Only if torsional rigidity could be maintained at the junctions between right- and left-handed helix would such structures be allowed by the present data.

The question of the existence of torsion joints in DNA's that have bound basic proteins and polycations is currently under investigation, as is the variation of the torsion elastic constant with temperature, pH, salt, and adsorbed polycations.

4. Conclusion

Neither the Initial Exponential Decay Zone formula nor the single-exponential-plus-baseline employed by Wahl et al. is capable of fitting the present data for a clean ϕ29 DNA over the full range of experimental time-spans with the same fixed set of parameters.

The present data are very well fit on all experimental time-spans by the Intermediate Zone formula with essentially the same set of parameters in every case. In addition, the variation in fitting parameters of the other formulas with experimental time-span can be rationalized in terms of Intermediate Zone relaxation of the FPA.

Evidently, this DNA is indistinguishable from a torsionally uniform elastic filament at the resolution of the present experiment, which is sufficient to guarantee that the linear density of torsion joints, if present, cannot lie in the range from 1 in every 20 base-pairs to about 1 in every 1000 base-pairs.

The torsional rigidity of this DNA is $C = 1.29 \pm 0.10 \times 10^{-19}$ cm^2 in 0.01 M NaCl at 25°C, somewhat smaller than previous estimates.

[1] S.A. Allison and J.M. Schurr, Chem. Phys. 41 (1979) 35.
[2] M.D. Barkley and B.H. Zimm, J. Chem. Phys. 70 (1979) 2991.
[3] Ph. Wahl, J. Paoletti and J.-B. LePecq, Proc. Natl. Acad. Sci. USA (1970) 417.
[4] J.C. Thomas, R.D. Holder, S.A. Allison and J.M. Schurr, Dynamic light scattering studies of internal motions in DNA. II. Clean viral DNA's, Biopolymers, in press.
[5] S.-C. Lin, S.A. Allison, J.C. Thomas and J.M. Schurr, Dynamic light scattering studies of internal motions in DNA. III. Evidence for titratable joints associated with bound polycations, Biopolymers, in press.
[6] J.C. Thomas and J.M. Schurr, Optics Lett. 4 (1979) 222.
[7] J.C. Thomas and J.M. Schurr, Dynamic light scattering studies of DNA. II. Effect of ionic strength on the structure and internal dynamics of viral ϕ29 DNA, Biopolymers 19 (1980) 215.
[8] D. Genest and Ph. Wahl, Biophys. Chem. 7 (1978) 317.
[9] G.R. Haugen, B.W. Wallin and F.E. Lytle, Rev. Sci. Instrum. 50 (1979) 64.
[10] S.K. Poultney, in: Advances in electronics and electron physics, ed. L. Marton (Academic, NY 1972) Chap. 2, p. 86.
[11] M. Maier, W. Kaiser and J.A. Giordmaine, Phys. Rev. Lett. 17 (1966) 1275.
[12] P.R. Bevington, Data reduction and error analysis for the physical sciences (McGraw-Hill, NY 1969).
[13] A. Grinvald and I.Z. Steinberg, Analytical Biochem. 59 (1974) 583.
[14] F. Perrin, J. Phys. Rad. 5 (1934) 497; 7 (1936) 1.
[15] R.E. De Pew and J.C. Wang, Proc. Natl. Acad. Sci. USA 72 (1975) 4275.
[16] D.E. Pulleybank, M. Shure, D. Tang, J. Vinograd and H.P. Vosberg, Proc. Natl. Acad. Sci. USA 72 (1975) 4280.
[17] A.H.-J. Wang, G.J. Quigley, F. J. Kolpak, J.L. Crawford, J.H. van Boom, G. vander Marel and A. Rich, Nature 282 (1979) 680.
[18] S. Arnott, R. Chandrasekharan, D.L. Birdsall, A.G.W. Leslie and R.L. Ratliffe, Nature 283 (1980) 743.